Yun *et al.*
Journal of Analytical Science and Technology (2024) 15:39
https://doi.org/10.1186/s40543-024-00453-1

Journal of Analytical Science and Technology

RESEARCH ARTICLE Open Access

NMR structure and functional studies of the fourth FAS1 domain of human periostin

Hyosuk Yun[1], Jeong-Eun Seon[2], Kon-Young Ji[2,4], Hye Jung Min[3*], Hyung-Sik Kang[2*] and Chul Won Lee[1*]

Abstract

Periostin is a matricellular protein that consists of several structural and functional domains, including EMILIN-like, four internal repeat fasciclin1 (FAS1) domains, and a carboxyl-terminal variable domain. It is known that periostin is associated with various fundamental biological processes and diseases, such as several types of cancer and chronic inflammatory diseases. Despite its important roles, the biological function of each domain is poorly understood. In this study, we expressed the fourth FAS1 (FAS1 IV) domain of human periostin, which was highly soluble and stable enough for structural and functional studies. The three-dimensional structure of FAS1 IV was determined using 3D NMR spectroscopy. The overall structure of FAS1 IV consists of six α-helices, one 3_{10} helix, and eight β-strands. Two triangular α-helical modules formed by three α-helices each are located on one side of the molecule, while the orthogonal β-sheet sandwich module of FAS1 IV is located on the other side. The isolated FAS1 IV domain exhibited cell invasion, migration, and adhesion activities for cancer cell lines comparable to those of the full FAS1 I–IV domain. In conclusion, we propose that the FAS1 IV domain is functionally active in human periostin and provides valuable information for understanding the biological function of periostin.

Keywords Nuclear magnetic resonance, Periostin, Extracellular matrix, FAS1 domain, Solution structure

Introduction

Periostin is an extracellular matrix protein that was originally identified in mesenchymal cells, such as osteoblasts, osteoblast-derived cells, and periodontal ligament cells (Bruder et al. 1998; Dorafshan et al. 2022; Horiuchi et al. 1999; Suzuki et al. 2004; Takeshita et al. 1993). Periostin has been found to be widely expressed in various tissues and organs, including the aorta, stomach, uterus, periodontal ligaments, cardiac valves, and breast (Gillan et al. 2002; Kruzynska-Frejtag et al. 2001; Tai et al. 2005). Periostin has at least two major biological roles; one is fibrillogenesis, which occurs in the matrix, and the other is cell migration (Kudo 2011). Periostin is also involved in many basic biological processes, including cell proliferation, cell invasion, and angiogenesis, and may also be involved in regulating a diverse set of cancer cell activities that contribute to tumorigenesis, cancer progression, and metastasis (Dorafshan et al. 2022; Li et al. 2015; Wang & Ouyang 2012). In addition, periostin has also been shown to be involved in chronic inflammatory diseases, such as atopic dermatitis and asthma (Kou et al. 2014; Masuoka et al. 2012; Parulekar et al. 2014). Periostin can activate both the Akt/PKB and FAK-mediated signaling pathways by interacting with integrins on cancer cells (Gillan et al. 2002; Mizejewski 1999; Varner and Cheresh 1996; Wang et al. 2022). Activation of these signaling cascades promotes cell survival, angiogenesis, invasion, metastasis,

*Correspondence:
Hye Jung Min
sarock@kwu.ac.kr
Hyung-Sik Kang
kanghs@jnu.ac.kr
Chul Won Lee
cwlee@jnu.ac.kr
[1] Department of Chemistry, Chonnam National University, Gwangju 61186, Republic of Korea
[2] School of Biological Sciences and Technology, Chonnam National University, Gwangju 61186, Republic of Korea
[3] Department of Cosmetic Science, Gwangju Women's University, Gwangju 62396, Republic of Korea
[4] KM Convergence Research Division, Korea Institute of Oriental Medicine, 1672 Yuseongdae-ro, Yuseong-gu, Daejeon 34054, Republic of Korea

and the epithelial-mesenchymal transition (Lafrenie & Yamada 1996; Morra and Moch 2011). High levels of expression of periostin have been detected in many solid tumors, and its expression correlates with tumor progression and cancer metastasis. Thus, in clinical practice, periostin can be considered to be both a biomarker and a therapeutic target allowing the detection and treatment of cancers, as well as chronic inflammatory diseases.

The FAS1 domains in periostin show significant homology to a protein named transforming growth factor β-induced protein (TGFβIp). This protein is associated with various corneal dystrophies and seems to play a role in cell adhesion (Michaylira et al. 2010; Takeshita et al. 1993; Ween et al. 2012). The FAS1 domains in periostin interact with several integrins on the cell surface (Kim et al. 2002; Moody and Williamson 2013), which are αβ heterodimeric receptors involved in cell–cell and cell-ECM interactions, and are associated with cellular attachment, migration, proliferation, survival, and differentiation (Kudo et al. 2007).

Periostin is a 90-kDa protein composed of an amino-terminal signal sequence, an EMILIN-like (EMI) domain, four internal repeat fasciclin1 (FAS1) domains, and a carboxyl-terminal variable domain (Fig. 1A) (Bruder et al. 1998; Horiuchi et al. 1999; Kudo 2011; Takeshita et al. 1993). The EMI domain, which is rich in cysteine, is involved in protein–protein interactions or protein multimerization under non-reducing conditions (Doliana et al. 2000). The four FAS1 domains are composed of approximately 150 amino acids each and share about 25% sequence identity (Litvin et al. 2005) and act as ligands for the integrin receptors αvβ3 and αvβ5, which initiate crosstalk with receptor tyrosine kinases such as EGFR and VEGF (Ghatak et al. 2014). The C-terminal variable domain undergoes alternative splicing, resulting in seven isoforms in humans that can be detected in various cancers, such as pancreatic, colon, and breast cancer (Bao et al. 2004; Baril et al. 2007; Grigoriadis et al. 2006; Hoersch and Andrade-Navarro 2010; Shao et al. 2004; Tai et al. 2005).

In this study, the FAS1 domains from human periostin were cloned and their expression was evaluated in an *E. coli* expression system. All the FAS1 domains were well expressed; however, only the FAS1 IV domain was suitable for the structure determination (Yun et al. 2018, 2016). The CD study showed that the FAS1 domains were composed of a mixture of α-helix and β-sheets. The three-dimensional structure of FAS1 IV was determined by 3D NMR spectroscopy using ^{15}N- or ^{13}C/^{15}N-labeled FAS1 IV domain. In addition, we examined the biological functions of the FAS1 domains using cell-based experiments with cancer cells. These functional studies indicated that the recombinant FAS1 IV domain can induce adhesion, migration, and invasion of cancer cell lines.

Results

Expression and purification of FAS1 IV domain

To investigate the structure and function of FAS1 domains of human periostin, we previously cloned various DNA constructs for FAS1 domains into an expression vector (Fig. 1B) and expressed using *E. coli* expression system (Yun et al. 2016). Among all four FAS1 domains, only FAS1 IV domain was highly soluble and showed a well-dispersed 2D ^{1}H-^{15}N HSQC

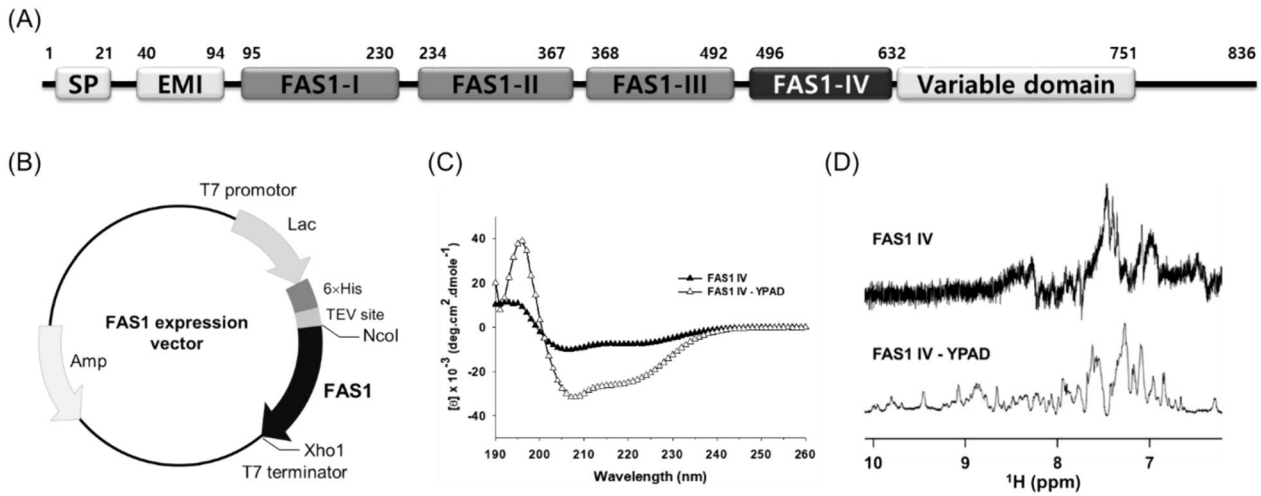

Fig. 1 Domain structure of human periostin (**A**), expression vector for FAS1 domains (**B**), circular dichroism spectra (**C**), and 1D proton NMR spectra of FAS1 IV domain (FAS1 IV and FAS1 IV-YPAD) (**D**). FAS1 IV-YPAD indicates that the YPAD sequence is attached to the C terminus of the FAS1 IV domain

spectrum (Yun et al. 2018). In this study, we revealed that the C-terminal YPAD sequence of the FAS1 IV domain was critical for the structure determination. With YPAD sequence, the FAS1 IV domain showed the enhanced intensities in CD and NMR spectra, and better peak dispersion in NMR spectrum, suggesting more soluble and rigid conformation with YPAD sequence at the C-terminal FAS1 IV domain (Fig. 1C, D). Therefore, we overexpressed the FAS1 IV with the C-terminal YPAD sequence for the structural and functional studies. The FAS1 IV was initially purified using a Ni-affinity chromatography, followed by dialysis, TEV cleavage, and a second Ni-affinity chromatography. The expression and purification steps were confirmed by SDS-PAGE analysis (Supplementary Fig. S1A). Further purification steps were performed using anion exchange and gel filtration chromatography to obtain highly pure FAS1 IV sample. The purity and molecular weight of the purified FAS1 IV was analyzed using ESI-LC-MS (Supplementary Fig. S1B and C).

NMR structure determination of FAS1 IV

The FAS1 IV domain of human periostin comprises residues 496–632 with three additional residues (Gly-Ala-Met) at the N terminus. All NMR spectra were recorded at 288 K. The ^{1}H-^{15}N HSQC spectrum revealed that the FAS1 IV domain was well folded in the NMR buffer based on the signal dispersion and homogenous intensity of the resonances showing almost peaks (153 peaks out of 156 theoretical peak number) (Supplementary Fig. S2). All 3D NMR experiments were performed at 288 K using Bruker Avance 700, 800, and 900 MHz spectrometers. More than 98% backbone resonances (^{1}H, ^{15}N, ^{13}Cα, and ^{13}C′) of FAS1 IV were sequentially assigned using 3D NMR spectroscopy including HNCA, HNCOCA, HNCACB, CBCACONH, and HNCO (Fig. 2), except for the two N-terminal residues, Gly574, Asn605, Glu606, and five prolines. Moreover, 93.2% of the observable side-chain resonances were assigned. The secondary structure constraints of the FAS1 IV domain were calculated using TALOS-N program based on the backbone HN, N, CA,

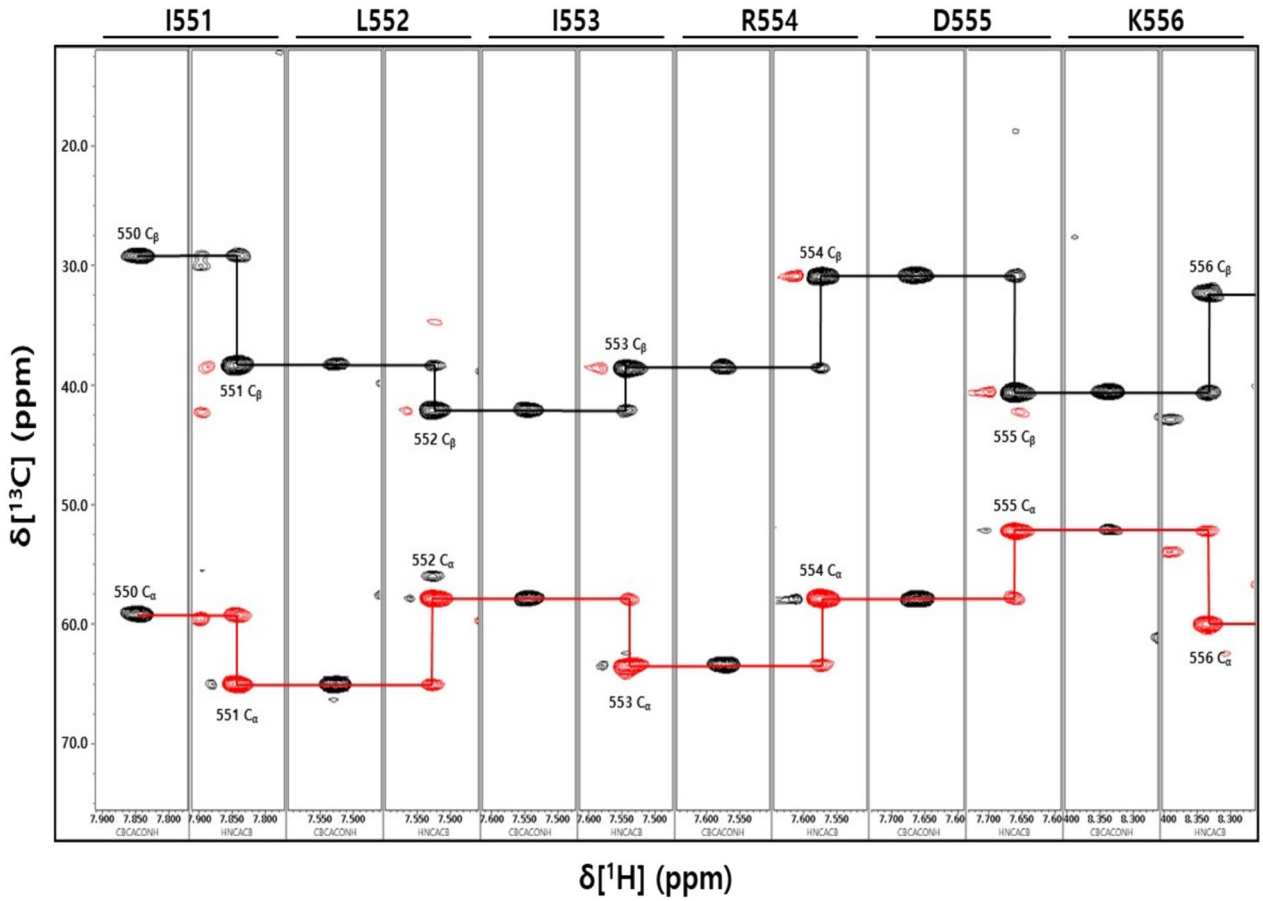

Fig. 2 Backbone sequential assignment process of FAS1 IV with CBCA(CO)NH and HNCACB spectra. CBCA(CO)NH spectrum indicates 2 peaks with i-1 (Cα, Cβ). HNCACB spectrum indicates 4 peaks with i-1 (Cα, Cβ) and i (Cα, Cβ). The peaks of own residue appear greater intensity and the peaks of proceeding residue appear weaker intensity

Table 1 NMR restraints and structural statistics for FAS1 IV domain

NMR restraints	
Nuclear Overhauser effect (NOE)-derived distance restraints	2596
Intraresidue (*i*, *i*)	865
Sequential (*i*, *i* + 1)	841
Medium-range ($2 \le \|i-j\| \le 4$)	654
Long-range ($\|i-j\| \ge 5$)	236
Hydrogen bond restraints	54
Dihedral angle restraints	196
Structural statics (23 structures)	
Violations	
Number of distance restraints > 0.5 Å	0
Number of dihedral angle restraints > 5°	0
Root-mean-square deviation (RMSD) from experiments	
Distance (Å)	0.050 ± 0.004
Dihedral angle (°)	0.775 ± 0.295
RMSD from idealized geometry	
Bonds (Å)	0.004 ± 0.000
Angles (°)	0.508 ± 0.025
Impropers (°)	0.356 ± 0.029
Ramachandran analysis (%) (all residues)	
Most favored region	89
Allowed region	8
Disallowed region	3
Average pairwise RMSD (Å) (residues 7–132)	
Backbone heavy atoms	0.99 ± 0.19
All heavy atoms	1.68 ± 0.22

CB, and C′ chemical shifts. The initial structures of FAS1 IV were calculated using CYANA and then the initial structure was further refined using Xplor-NIH. The NMR restraints and structural statistics for FAS1 IV are summarized in Table 1. The structure of FAS1 IV domain was deposited at RCSB databank (PDB ID 5WT7).

Structural description of FAS1 IV

The final 23 structures of FAS1 IV with the lowest energy were selected from the 100 refined structures. The average pairwise RMSD values of backbone and heavy atoms are 0.99 ± 0.19 Å and 1.68 ± 0.22 Å, respectively (Table 1). The overall structure of FAS1 IV exhibited a globular and rigid fold except for both terminal regions and a short loop between α4 and α5 helix (Fig. 3B). The secondary structure of FAS1 IV is composed of six α-helices, one 3_{10} helix, and eight β-strands: α-helices (α1, L499-Q505; α2, S510-A518; α3, K522-T526; α4, N538-F541; α5, S546-I553; α6, K556-I563), one 3_{10} helix (K507-F509), and eight β-strands (β1, W531-P536; β2, T568-P569; β3, N583-K586; β4, K592-V598; β5, T601-V604; β6, L607-K608; β7, E611-S612; β8, G619-V624) (Fig. 3A, C). Two triangular α-helical modules formed by three α-helices each (α1, α2, and α3; α4, α5, and α6, respectively) are located in one side of the molecule (Fig. 3C, D). The orthogonal β-sheet sandwich module of FAS1 IV is located at the other side of the molecule. The β-sandwich module is composed of two β-sheets. One is composed of three β-strands (β2-β1-β8-β7) in the core of the structure, and the other is formed by three β-strands (β3-β4-β5-β6) exposed to solvent. The two β-sheets are

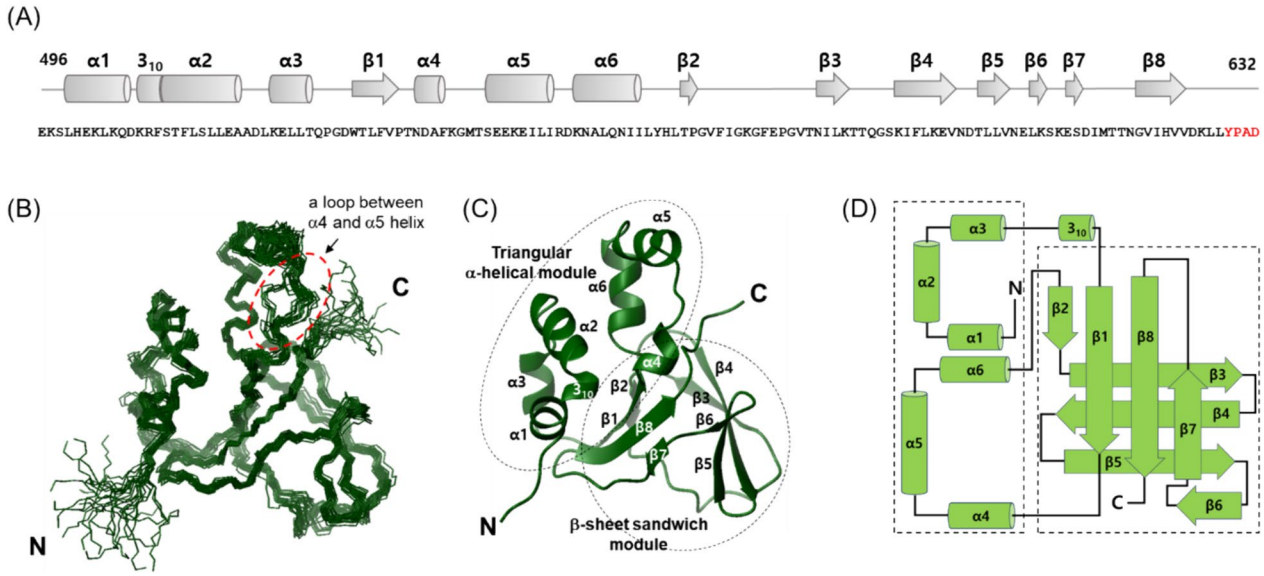

Fig. 3 Primary sequence and NMR solution structure of FAS1 IV domain of human periostin (PDB ID 5WT7). **A** Primary and secondary structure of FAS1 IV domain. Line (**B**) and ribbon (**C**) structures of FAS1 domain. **D** Secondary structure topology of FAS1 IV domain. Secondary structures were labeled and structural modules were indicated by dotted circles

almost perpendicular to one another (Fig. 3D). The two triangular α-helical modules are connected through the β1 strand and then the orthogonal β-sandwich module is connected through a relatively long loop between β2 and β3 strand.

Structure comparison of FAS1 domains

The crystal structure of human periostin construct containing EMI and full FAS1 domains (FAS1 I to IV) was reported (Liu et al. 2018). The full-length structure suggested that periostin exists as a dimer in solution mediated by EMI domain. Without EMI domain, the full FAS1 I to IV can exist as an independent and stable module. The NMR solution structure of FAS1 IV determined in this study is well superimposed with the crystal structure of human periostin FAS1 IV domain (Fig. 4A). The overall secondary structures are well conserved with small variations. For instance, the additional β-strand 6 and 7 between two orthogonal β-sheet sandwich modules were detected in the NMR structure. In addition, the helix packing in the triangular α-helix module is not well converged between NMR and X-ray structures of FAS1 IV domain (Fig. 4A). These structural differences probably result from the differences in solution and crystal state of the samples or from the different construct of samples (FAS1 IV vs full FAS1-I to IV between NMR and crystal structures). The crystal structure of TGFβIp EMI-FAS1 I-IV has been reported (Garcia-Castellanos et al. 2017). The primary and tertiary structures of FAS1 IV domains of periostin and TGFβIp are highly homologous (sequence identity = 37.5%) with subtle differences in the length of secondary structures (Fig. 4B, C). The β-strand 6 and 7 between two orthogonal β-sheet sandwich modules were slightly different and the helix orientation in the triangular α-helix module is also little bit different between periostin and TGFβIp.

Cell-based activity of FAS1 IV domain

Periostin has been known to promote cell survival, angiogenesis, adhesion, proliferation, migration, and invasion by interacting with the αvβ3 and αvβ5 integrins of several cancer cell lines (Michaylira et al. 2010). Therefore, we investigated the activities of the recombinant FAS1 domains on the metastatic potential for human colon cancer HCT116 and breast cancer MCF7 cell lines using in vitro cell-based experiments including adhesion, migration, and invasion assays (Fig. 5 and Supplementary Fig. S3).

The recombinant FAS1 IV domain efficiently enhanced the adhesion of the colon cancer HCT116 cells in a

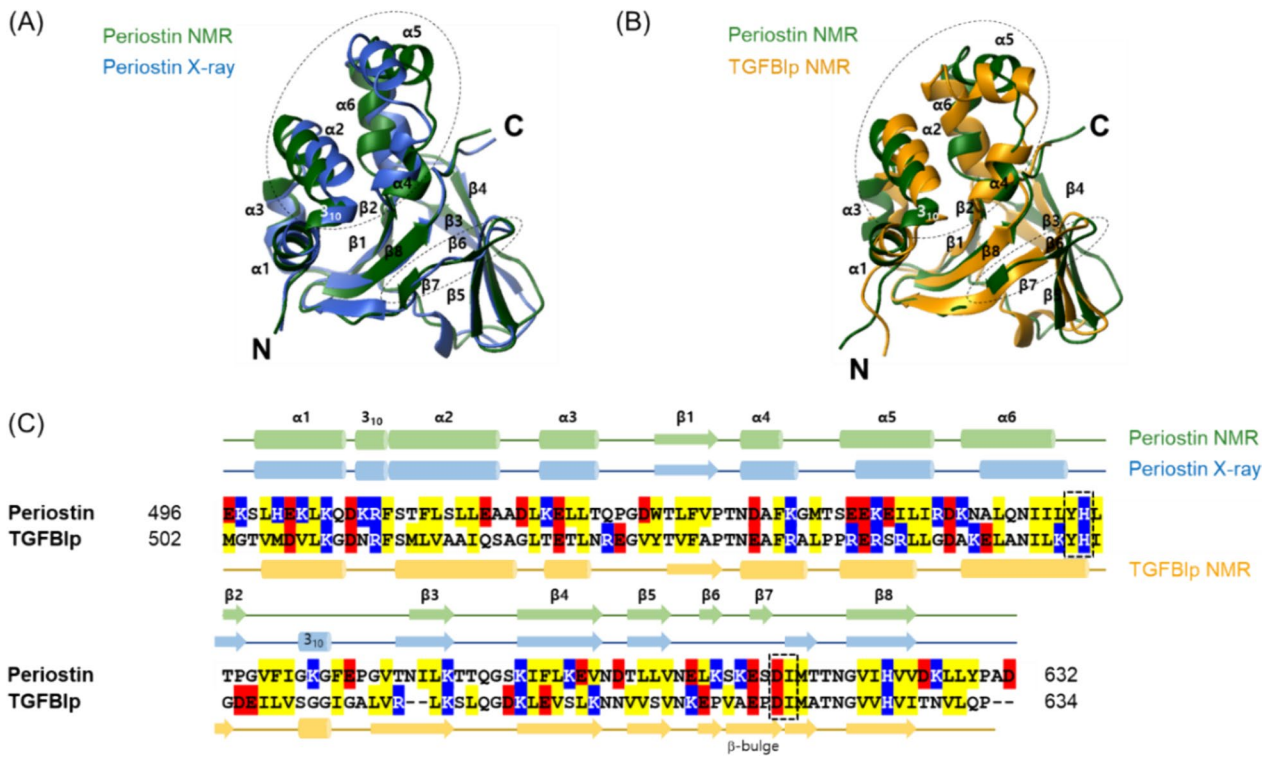

Fig. 4 Structure comparison of FAS1 domains. **A** Superimposition of the NMR and X-ray (PDB ID 5YJH) structure of FAS1 domain of human periostin. **B** Superimposition of the FAS1 domain of periostin and TGFβIp (PDB ID 2LTB). **C** Sequence alignment of FAS1 domains of periostin and TGFβIp

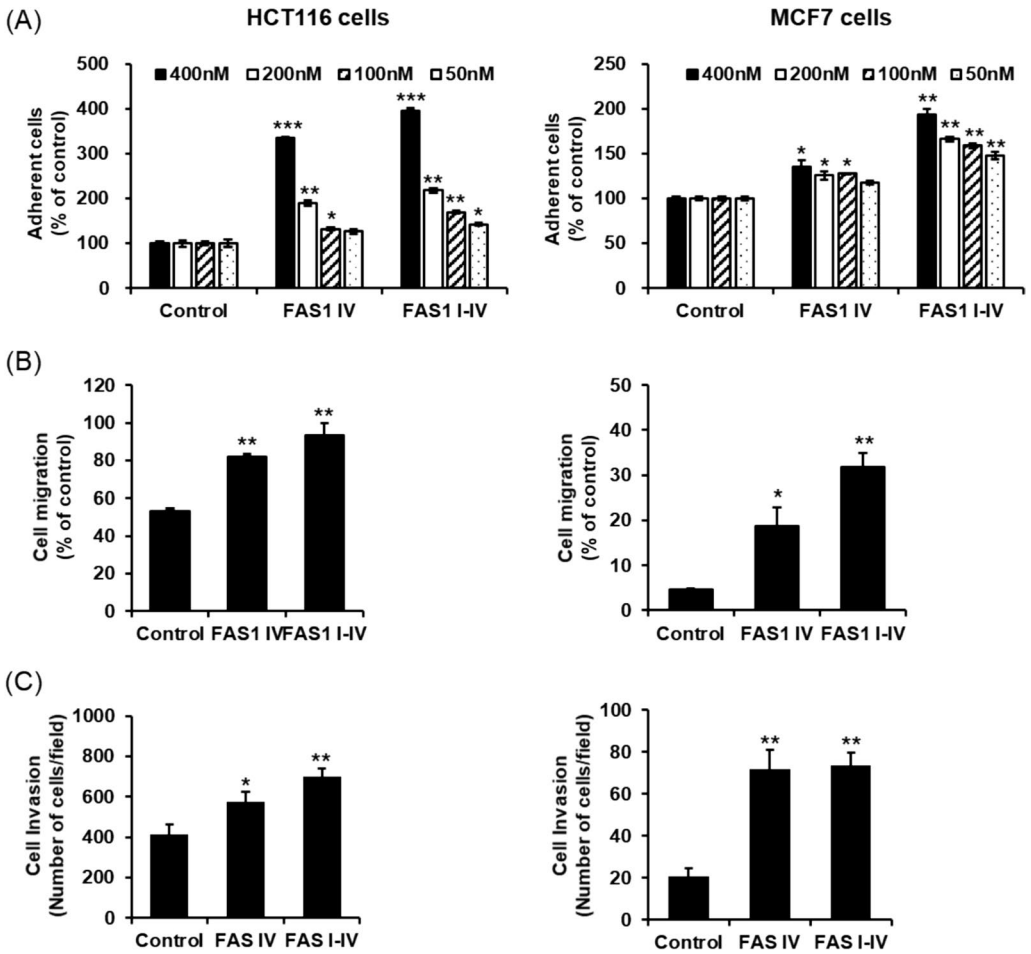

Fig. 5 Effects of the periostin FAS1 domains on adhesion and wound healing assay. Dose-dependent effects of adhesion (**A**), cell migration (**B**), and cell invasion **C** of FAS1 domains were determined with HCT116 and MCF7 cells

dose-dependent manner up to 340% compared to the bovine serum albumin (BSA) as a negative control, which is almost 85% of that of full FAS1 I-IV domain (400% compared to control) (Fig. 5A). These results imply that the single FAS1 IV domain has a potential adhesion activity comparable to full FAS1 I-IV domain for HCT116 cells. In case of MCF7 cells, FAS1 domain induced cell adhesion but not high induction as HCT116 cells (140 and 195% compared to control for FAS1 IV and FAS I-IV, respectively). In addition, the cell migration and invasion activities of HCT116 and MCF7 cells were also increased by FAS1 IV or full FAS1 I-IV domains (Fig. 5B, C).

Discussion

The human periostin protein is composed of multiple functional domains including four FAS1 domains that play important roles in cell adhesion and tumor metastasis by interacting with integrins. Despite their important biological role, the functionally important site of the periostin FAS1 domains has not been revealed yet. Previously, we suggested that the single FAS1 IV domain of human periostin is highly soluble and suitable for studying its structural and functional properties compared to other periostin FAS1 domains (Yun et al. 2018, 2016). In this study, we determined the NMR structure of FAS1 IV domain of human periostin and reported a functional site on this domain. Among four FAS1 domains, the FAS1 IV was most suitable for NMR study, as it was the only domain that showed high solubility and a well-dispersed 2D ^{1}H-^{15}N HSQC spectrum. Interestingly, the C-terminal 4 residues (YPAD) are critical for forming a stable conformation. Although a stable conformation of the C-terminal YPAD was not clearly defined due to insufficient NMR constraints in this region, the determined ensemble structure contained many conformers that support considerable interaction of the YPAD with a hydrophobic surface pocket in FAS1 IV (Supplementary Fig. S4). Therefore,

it is plausible that the YPAD could enhance the overall stability of the FAS1 IV structure in solution by interfering with undesirable hydrophobic surface interactions of the domain, even though the YPAD contacts may occur transiently.

Several structures of FAS1 domains have been determined. The structure of the fourth FAS1 domain from TGFβIp has been solved using both NMR and X-ray crystallography (Garcia-Castellanos et al. 2017; Underhaug et al. 2013). Additionally, the NMR structure of Fdp (Fasciclin I Domain Protein) from Rhodobacter sphaeroides, and the crystal structure of FASI III-IV from Drosophila melanogaster have been solved (Clout et al. 2003; Moody & Williamson 2013). Furthermore, the structures of other proteins with a homologous fold to the FAS1 domain have been solved using NMR, including the CupS from *Thermosynechococcus elongatus* and the MPB70 protein from *Mycobacterium tuberculosis* (Carr et al. 2003; Korste et al. 2015). The structure of TGFβIp was also determined by X-ray crystallography (PDB ID 5NV6), including the structure of the EMI-like domain (CROPT, Cysteine-Rich domain Of Periostin and TGFβIp) and four FAS1 domains. The primary sequence of the EMI domain of periostin shows high similarity to that of the CROPT domain in TGFβIp, and the locations of all the cysteine residues are conserved, suggesting that the structure of the EMI domain in periostin is very similar to that in TGFβIp.

The FAS1 domain has been found in many other proteins across various living organisms, including bacteria, plants, animals, and humans. For example, the bacterial immunogenic protein MPT70 contains one FAS1 domain, and human TGFβIp and periostin contain tandem repeats of four homologous FAS1 domains. In particular, the integrin binding residues (YH and DI sequences) in TGFβIp are conserved in the sequence of periostin FAS1 IV domain (Fig. 4C, dotted rectangles), implying that the independent FAS1 IV domain of periostin is biologically important. To examine the functions of the FAS1 IV domain, we performed cell-based experiments, including cell adhesion, migration, and invasion assays, using colon and breast cancer cell lines (Fig. 5). The presence of the FAS1 IV domain effectively increased the activity against both cell lines. The structure of human periostin, including the EMI and FAS1 I–IV domains, was solved by X-ray crystallography (Liu et al. 2018). This paper reported that human periostin predominantly exists as a dimer through homophilic interactions between periostin domains. Although the complex structure of periostin domains may be involved in its fully functional activity, the single FAS1 IV domain also showed effective activity comparable to the full FAS1 I-IV domain in vitro experiments.

Conclusion

Periostin is an important protein associated with various diseases, such as cancer metastasis and allergies. However, the biological function of FAS1 domains has remained unknown. In this study, we successfully expressed and purified the stable and independent FAS1 IV domain of human periostin. Using 3D NMR spectroscopy, we determined the tertiary structure of FAS1 IV, which exhibited a well-folded tertiary structure with high similarity to the full FAS1 I-IV domain, but with subtle differences in local structure.

Notably, the FAS1 IV domain demonstrated cell migration, adhesion, and invasion activity against cancer cell lines, which was comparable to the full FAS1 I-IV domain. These findings strongly suggest that the FAS1 IV domain holds significant potential as an important target for studying the biological function and potential applications of human periostin in various contexts.

Materials and methods

Expression of FAS1 domains of periostin

Four DNA constructs encoding the FAS1 I, II, III, and IV domains of human periostin (Fig. 1A) were cloned into the pHIS2 vector using NcoI and XhoI restriction enzymes (Fig. 1B). The expression vector contains an N-terminal hexa-histidine tag, followed by a tobacco etch virus (TEV) protease cleavage site. PCR amplification of the DNA encoding the FAS1 domains was performed using the polymerase chain reaction (PCR). The DNA polymerase Pfu Plus and a PCR master mix was used to amplify the PCR products using the following 30 temperature cycles; denaturation at 94 °C for 30 s, followed by annealing and extension. The resultant PCR products were purified using a PCR product purification kit and digested at 37 °C for 20 min and then analyzed by 1% (w/v) agarose gel electrophoresis. The digested products were purified using a gel extraction kit and treated with T4 DNA ligase for ligation at room temperature for 1 h. The ligated products were then transformed into competent DH5α cells.

The expression vectors containing the different recombinant constructs were confirmed by DNA sequencing and transformed separately into *E. coli* BL21 (DE3) and cultured at 37 °C in 1 L LB media supplemented with 100 μg/mL ampicillin. When the optical density at 600 nm reached 0.6, the culture was moved from 37 to 15 °C, and FAS1 domain expression was induced for 20 h in the presence of 0.5 mM IPTG. For the stable isotope labeling of FAS1 domain, the cell was cultured in M9 minimal medium supplemented with $^{15}NH_4Cl$ or $^{15}NH_4Cl$ and ^{13}C-Glucose. The culture was harvested by centrifugation at 4000 rpm at 4 °C for 30 min, and the

pellet resuspended in lysis buffer comprised of 20 mM imidazole, 20 mM β-mercaptoethanol, 0.5 M NaCl, and 20 mM Tris–HCl (pH 8.0) and disrupted by ultrasonication for 20 min with a pulse of 1 s using a 3-s gap between pulses. The lysate was separated into pellet and supernatant by centrifugation at 25,000 g-force at 4 °C for 30 min. All expressed proteins were analyzed using SDS-PAGE to assess their expression and solubility.

Purification of FAS1 IV domain of periostin

The FAS1 IV domain of periostin was expressed and purified as described previously (Yun et al. 2018). Briefly, the supernatant of cell lysate was loaded onto the Ni–NTA agarose column (5 mL), and then the column was washed with 25 mL of lysis buffer (20 mM Tri-HCl (pH 8.0), 10 mM NaCl). The bound His-tagged FAS1 IV was stepwise eluted with 50, 100, 150, 200, 250, and 300 mM imidazole in lysis buffer. The eluted proteins were then dialyzed in 20 mM Tri-HCl (pH 8.0), 10 mM NaCl, and 20 mM β-mercaptoethanol for 4 h at 4 ℃. The dialyzed proteins were treated with the TEV protease at 4 °C for 16 h to remove the N-terminal His-tag. To further purify the proteins, the cleaved proteins were subjected to a second His-tag affinity chromatography step, and the unbound proteins were then purified further using a HiTrap Q anion exchange column with linear gradient from 0 to 500 mM NaCl in buffer A containing 0.1 mM PMSF and 1 mM EDTA. The final purification was performed by gel filtration chromatography using a HiPrep 16/60 Sephacryl column (particle size: 47 μm) using 10 mM NaH_2PO_4 (pH 7.0), 50 mM NaCl, 0.1 mM PMSF, and 1 mM EDTA. The purified FAS1 IV domain was then concentrated using an Amicon ultra-15 Ultracel-3 K membrane.

LC–MS analysis

To determine the accurate molecular weight of the purified FAS1 IV domain, the protein was diluted to a final protein concentration of 45 μM in 15% acetonitrile (with 0.05% TFA). The protein was then analyzed using ESI-LC-MS (RP-HPLC, Shimadzu 10ADvp; API2000, AB Sciex) using a preparative ACE5 C18-300 Å (50 × 2.1 mm, 5 μm) column with a gradient from 5 to 95% acetonitrile for 15 min at a flow rate of 0.5 mL/min. The masses of samples were obtained in positive ion mode at mass ranges from 200 to 1800 *m*/*z*.

NMR spectroscopy

All NMR experiments were performed at 288 K using Bruker Avance 700, 800, and 900 MHz spectrometers at the Korea Basic Science Institute (KBSI). NMR samples were prepared in10% D_2O/90% H_2O or 100% D_2O containing10 mM NaH_2PO_4 (pH 7.0), 50 mM NaCl, 10 μM DSS, and 0.04% NaN_3. Backbone resonance assignments were obtained from 3D HNCA (Grzesiek and Bax 1992), HN(CO)CA, HNCACB (Wittekind and Mueller 1993), CBCA(CO)NH (Grzesiek & Bax 1992), and HNCO (Kay et al. 1990). Sidechain resonance assignments were based on 3D CCH-TOCSY, HCCH-COSY, and HCCH-TOCSY (Bax et al. 1990). In addition, ^{1}H-^{13}C HSQC (Palmer et al. 1991), ^{13}C-NOESY-HSQC, ^{15}N-TOCSY-HSQC, and ^{15}N-NOESY-HSQC (Marion et al. 1989; Zuiderweg and Fesik 1989) were used for the sidechain assignment and NOE restraints. All NMR spectra were processed and analyzed using the programs NMRPipe (Delaglio et al. 1995) and NMRViewJ (Johnson and Blevins 1994).

Three-dimensional structure calculation

NOEs were automatically assigned by CYANA 2.1 (Guntert 2004) during the initial structure calculation. The backbone torsion angle restraints were obtained from TALOS-N (Shen and Bax 2013) calculation. The CYANA structures were refined by Xplor-NIH 3.8 (Schwieters et al. 2003), supplemented with hydrogen bond restraints for the α-helix and β-strand regions of FAS1 IV at a later stage. After iterative refinement, incorrect and ambiguous assignments were removed. Finally, 100 structures were calculated in the final iteration, and the 23 lowest energy structures were selected. The 23 NMR structures of FAS1 IV have been deposited to Protein Data Bank (accession code 5WT7). The final 23 structures were analyzed, and figures were prepared using MOLMOL (Koradi et al. 1996) and Pymol (Schrodinger 2015).

Refolding of FAS1 full domain

The expressed FAS1 full domain (FAS1 I-IV) went to inclusion body inside *E. coli* cells. Therefore, we refolded the FAS1 full domain from the inclusion body using rapid dilution method. In brief, cells were harvested by centrifugation and resuspended in 2 × PBS (pH 7.4) containing 2 mM DTT and lysed by sonication. The inclusion bodies were collected by centrifugation at 15,000 rpm at 4 °C for 30 min. The inclusion bodies were resuspended in 8 M urea containing 0.5 M β-mercaptoethanol. The resuspended inclusion bodies were then induced to resolubilize by diluting in refolding buffer [20 mM Tris (pH 8.0), 0.5 M NaCl, 20 mM imidazole, and 20 mM β-mercaptoethanol] and stirred for 24 h at 4 °C. After centrifugation, the solubilized FAS1 full domain was loaded onto an Ni–NTA column and the bound protein was eluted with 0.3 M imidazole in refolding buffer. For further purification, the eluted FAS1 full domain was concentrated and loaded into a HiPrep 16/60 gel filtration column with 1 × PBS (pH 7.4) buffer containing 0.5 mM DTT. The purified FAS1 full domain protein was

concentrated using a 3000 MWCO Amicon Ultra centrifugal filter device before use.

Mammalian cell culture

The MCF7 human breast cancer and HCT116 human colon cancer cells were cultured and maintained at 37 °C in 5% CO_2 in Dulbecco's modified Eagle's medium (DMEM) containing 10% fetal bovine serum supplemented with antibiotics. The cells were seeded at a density of 5×10^5 cells in 10 cm diameter culture dishes. After 3 days, the cells were trypsinized and counted using a hemocytometer. All cell-based experiments were performed in triplicate, and controls were used to assess non-specific binding.

Cell adhesion assay

Cell adhesion assay was performed in 96-well ELISA plates coated at 4 °C overnight with all protein samples at concentrations of 50, 100, 200, or 400 nM, respectively. The plates were blocked by incubation with 2% bovine serum albumin (BSA) for 1 h at 37 °C. The cells were then trypsinized and resuspended in medium at a density of 5×10^5 cells/mL MCF7 or HCT116 cells. After that, 0.1 mL of the prepared cell suspensions were added to each well and incubated for 1 h at 37 °C. Non-adherent cells were removed by gently rinsing three times with 0.2 mL PBS. Adherent cells were quantitated by determining the absorbance at 450 nm using EZ-CYTOX (Dogenbio, Seoul, Republic of Korea) according to the manufacturer's instructions.

Cell migration assay

Flat-bottomed 96-well plates were coated with either 500 nM of FAS1 IV or FAS1 I-IV domain overnight at 4 ℃. The coated plates were washed twice with 0.2 mL PBS, after which 0.1 mL of cell suspension of MCF7 cells or HCT116 cells (5×10^4 cells/mL) were added to the protein coated plates for 24 h at 37 ℃ in an atmosphere of 5% CO_2. The cell monolayers were gently and slowly scratched with a 1-mL pipette tip across the center of the wells. The wells were gently washed with medium to remove the detached cells and a further 0.1 mL of DMEM was added to each well. The plates were incubated for a further 48 h at 37 ℃ in an atmosphere of 5% CO_2. Wound confluence was measured using images of the cell wound by measuring the distance of the scratch wound at baseline to the distance of the scratch wound confluence at 100× magnification. The experiments were repeated three times.

Cell invasion assay

Cell invasion assay was performed using Matrigel transwell plates (8 μM; Corning Life Sciences, Corning, NY, USA) as an upper chamber and 24-well culture plates as a lower chamber (Kim et al. 2019). After coating of the upper chambers with 1 mg/mL of Matrigel for 2 h at 37 °C, HCT116 and MCF7 cells were added to the upper chamber at a density of 2×10^5 cells/well. The lower chambers were treated with 500 nM of FAS1 IV or FAS I-IV followed by incubated for 18 h in HCT116 cells and 72 h in MCF7 cells at 37 °C. After removal of the non-invaded cells using a cotton swab in the upper chamber, the invaded cells into the lower chamber were fixed with 4% paraformaldehyde and stained with hematoxylin and eosin.

Statistical analysis

For the statistical analyses of the data, P-values were calculated using one-way or two-way analysis of variance (ANOVA) and Student's *t* test. The results were considered statistically significant when *P*-values were <0.05.

Supplementary Information

The online version contains supplementary material available at https://doi.org/10.1186/s40543-024-00453-1.

Additional file 1: **Fig. S1**. Expression and purification of FAS1 IV domain of human periostin. (A) SDS-PAGE analysis of each purification step of FAS1 IV domain. RP-HPLC (B) and ESI-MS (C) analysis of finally purified FAS1 IV domain. **Fig. S2**. 1H-15N HSQC spectrum of the FAS1 IV domain of human periostin. **Fig. S3**. Effects of the periostin FAS1 domains on adhesion and wound healing assay. Dose-dependent effects of adhesin (A), cell migration (B), and cell invasion (C) of FAS1 domains were determined with HCT116 and MCF7 cells. **Fig. S4**. The surface structure of FAS1 IV domain with the C-terminal YPAD sequence. The YPAD residues were colored in red and labeled.

Acknowledgements

Not applicable.

Author contributions

CWL contributed to conceptualization, methodology, validation, investigation, data curation, writing—original draft, and visualization. HY contributed to methodology, validation, investigation, data curation, writing—original draft, and visualization. J-ES contributed to data curation and investigation. K-YJ contributed to data curation and investigation. HJM contributed to conceptualization and methodology. H-SK contributed to investigation, and visualization, data curation, supervision, and writing—review & editing. All authors read and approved the final manuscript.

Funding

This work was supported by the Basic Science Research Program through the National Research Foundation of Korea (NRF) funded by the Ministry of Education, Science, and Technology of Korea (NRF-2018R1D1A1B07043540 and NRF-2023R1A2C1007203 to CWL) and by Gwangju Women's University (KWU23-049 to HJM).

Availability of data and materials

The datasets used and/or analyzed during the current study available from the corresponding author on reasonable request. The datasets generated and/or analyzed during the current study are available in the GenBank, https://www.ncbi.nlm.nih.gov/nuccore/OR399556.

Declarations

Competing interests

No potential conflicts of interest relevant to this article exist.

Received: 1 May 2024 Accepted: 10 June 2024
Published online: 18 June 2024

References

Bao SD, Ouyang G, Bai XF, Huang Z, Ma CY, Liu M, Shoo R, Anderson RM, Rich JN, Wang XF. Periostin potently promotes metastatic growth of colon cancer by augmenting cell survival via the Akt/PKB pathway. Cancer Cell. 2004;5(4):329–39. https://doi.org/10.1016/S1535-6108(04)00081-9.

Baril P, Gangeswaran R, Mahon PC, Caulee K, Kocher HM, Harada T, Zhu M, Kalthoff H, Crnogorac-Jurcevic T, Lemoine NR. Periostin promotes invasiveness and resistance of pancreatic cancer cells to hypoxia-induced cell death: role of the beta(4) integrin and the PI3k pathway. Oncogene. 2007;26(14):2082–94. https://doi.org/10.1038/sj.onc.1210009.

Bax A, Clore GM, Gronenborn AM. 1H–1H correlation via isotropic mixing of 13C magnetization, a new three-dimensional approach for assigning 1H and 13C spectra of 13C-enriched proteins. J Magn Reson. 1990;88:425–31.

Bruder SP, Ricalton NS, Boynton RE, Connolly TJ, Jaiswal N, Zaia J, Barry FP. Mesenchymal stem cell surface antigen SB-10 corresponds to activated leukocyte cell adhesion molecule and is involved in osteogenic differentiation. J Bone Miner Res. 1998;13(4):655–63. https://doi.org/10.1359/jbmr.1998.13.4.655.

Carr MD, Bloemink MJ, Dentten E, Whelan AO, Gordon SV, Kelly G, Frenkiel TA, Hewinson RG, Williamson RA. Solution structure of the Mycobacterium tuberculosis complex protein MPB70: from tuberculosis pathogenesis to inherited human corneal desease. J Biol Chem. 2003;278(44):43736–43. https://doi.org/10.1074/jbc.M307235200.

Clout NJ, Tisi D, Hohenester E. Novel fold revealed by the structure of a FAS1 domain pair from the insect cell adhesion molecule fasciclin I. Structure. 2003;11(2):197–203.

Delaglio F, Grzesiek S, Vuister GW, Zhu G, Pfeifer J, Bax A. NMRPipe: a multidimensional spectral processing system based on UNIX pipes. J Biomol NMR. 1995;6(3):277–93.

Doliana R, Bot S, Bonaldo P, Colombatti A. EMI, a novel cysteine-rich domain of EMILINs and other extracellular proteins, interacts with the gC1q domains and participates in multimerization. FEBS Lett. 2000;484(2):164–8. https://doi.org/10.1016/s0014-5793(00)02140-2.

Dorafshan S, Razmi M, Safaei S, Gentilin E, Madjd Z, Ghods R. Periostin: biology and function in cancer. Cancer Cell Int. 2022;22(1):315. https://doi.org/10.1186/s12935-022-02714-8.

Garcia-Castellanos R, Nielsen NS, Runager K, Thogersen IB, Lukassen MV, Poulsen ET, Goulas T, Enghild JJ, Gomis-Ruth FX. Structural and functional implications of human transforming growth factor beta-induced protein, TGFBIp, in Corneal Dystrophies. Structure. 2017;25(11):1740–50. https://doi.org/10.1016/j.str.2017.09.001.

Ghatak S, Misra S, Norris RA, Moreno-Rodriguez RA, Hoffman S, Levine RA, Hascall VC, Markwald RR. Periostin induces intracellular cross-talk between kinases and hyaluronan in atrioventricular valvulogenesis. J Biol Chem. 2014;289(12):8545–61. https://doi.org/10.1074/jbc.M113.539882.

Gillan L, Matei D, Fishman DA, Gerbin CS, Karlan BY, Chang DD. Periostin secreted by epithelial ovarian carcinoma is a ligand for $\alpha_V\beta_3$ and $\alpha_V\beta_5$ integrins and promotes cell motility. Cancer Res. 2002;62(18):5358–64.

Grigoriadis A, Mackay A, Reis JS, Steele D, Iseli C, Stevenson BJ, Jongeneel CV, Valgeirsson H, Fenwick K, Iravani M, Leao M, Simpson AJG, Strausberg RL, Jat PS, Ashworth A, Neville AM, O'Hare MJ. Establishment of the epithelial-specific transcriptome of normal and malignant human breast cells based on MPSS and array expression data. Breast Cancer Res. 2006. https://doi.org/10.1186/Bcr1604.

Grzesiek S, Bax A. Improved 3D triple-resonance NMR techniques applied to a 31 kDa protein. J Magn Reson. 1992;96:432–40.

Guntert P. Automated NMR structure calculation with CYANA. Methods Mol Biol. 2004;278:353–78.

Hoersch S, Andrade-Navarro MA. Periostin shows increased evolutionary plasticity in its alternatively spliced region. BMC Evol Biol. 2010;10:30. https://doi.org/10.1186/1471-2148-10-30.

Horiuchi K, Amizuka N, Takeshita S, Takamatsu H, Katsuura M, Ozawa H, Toyama Y, Bonewald LF, Kudo A. Identification and characterization of a novel protein, periostin, with restricted expression to periosteum and periodontal ligament and increased expression by transforming growth factor beta. J Bone Miner Res. 1999;14(7):1239–49. https://doi.org/10.1359/jbmr.1999.14.7.1239.

Johnson BA, Blevins RA. NMR view: a computer program for the visualization and analysis of NMR data. J Biomol NMR. 1994;4(5):603–14. https://doi.org/10.1007/BF00404272.

Kay LE, Ikura M, Tschudin R, Bax A. Three-dimensional triple-resonance NMR spectroscopy of isotopically enriched proteins. J Magn Resonan. 1990;89:496–514.

Kim JE, Jeong HW, Nam JO, Lee BH, Choi JY, Park RW, Park JY, Kim IS. Identification of motifs in the fasciclin domains of the transforming growth factor-beta-induced matrix protein betaig-h3 that interact with the alphavbeta5 integrin. J Biol Chem. 2002;277(48):46159–65. https://doi.org/10.1074/jbc.M207055200.

Kim SM, Kim EM, Ji KY, Lee HY, Yee SM, Woo SM, Yi JW, Yun CH, Choi H, Kang HS. TREM2 acts as a tumor suppressor in colorectal carcinoma through Wnt1/beta-catenin and erk signaling. Cancers (basel). 2019;11(9):55. https://doi.org/10.3390/cancers11091315.

Koradi R, Billeter M, Wuthrich K. MOLMOL: a program for display and analysis of macromolecular structures. J Mol Graph. 1996;14(1):51–5.

Korste A, Wulfhorst H, Ikegami T, Nowaczyk MM, Stoll R. Solution structure of the NDH-1 complex subunit CupS from Thermosynechococcus elongatus. Biochim Biophys Acta. 2015;1847(10):1212–9. https://doi.org/10.1016/j.bbabio.2015.05.003.

Kou K, Okawa T, Yamaguchi Y, Ono J, Inoue Y, Kohno M, Matsukura S, Kambara T, Ohta S, Izuhara K, Aihara M. Periostin levels correlate with disease severity and chronicity in patients with atopic dermatitis. Br J Dermatol. 2014;171(2):283–91. https://doi.org/10.1111/bjd.12943.

Kruzynska-Frejtag A, Machnicki M, Rogers R, Markwald RR, Conway SJ. Periostin (an osteoblast-specific factor) is expressed within the embryonic mouse heart during valve formation. Mech Dev. 2001;103(1):183–8. https://doi.org/10.1016/S0925-4773(01)00356-2.

Kudo A. Periostin in fibrillogenesis for tissue regeneration: periostin actions inside and outside the cell. Cell Mol Life Sci. 2011;68(19):3201–7. https://doi.org/10.1007/s00018-011-0784-5.

Kudo Y, Siriwardena BS, Hatano H, Ogawa I, Takata T. Periostin: novel diagnostic and therapeutic target for cancer. Histol Histopathol. 2007;22(10):1167–74. https://doi.org/10.14670/HH-22.1167.

Lafrenie RM, Yamada KM. Integrin-dependent signal transduction. J Cell Biochem. 1996;61(4):543–53. https://doi.org/10.1002/(SICI)1097-4644(19960616)61:4%3c543::AID-JCB7%3e3.0.CO;2-O.

Li W, Gao P, Zhi Y, Xu W, Wu Y, Yin J, Zhang J. Periostin: its role in asthma and its potential as a diagnostic or therapeutic target. Respir Res. 2015;16(1):57. https://doi.org/10.1186/s12931-015-0218-2.

Litvin J, Zhu S, Norris R, Markwald R. Periostin family of proteins: therapeutic targets for heart disease. Anat Rec A Discov Mol Cell Evol Biol. 2005;287(2):1205–12. https://doi.org/10.1002/ar.a.20237.

Liu J, Zhang J, Xu F, Lin Z, Li Z, Liu H. Structural characterizations of human periostin dimerization and cysteinylation. FEBS Lett. 2018;592(11):1789–803. https://doi.org/10.1002/1873-3468.13091.

Marion D, Driscoll PC, Kay LE, Wingfield PT, Bax A, Gronenborn AM, Clore GM. Overcoming the overlap problem in the assignment of 1H NMR spectra of larger proteins by use of three-dimensional heteronuclear 1H–15N Hartmann-Hahn-multiple quantum coherence and nuclear Overhauser-multiple quantum coherence spectroscopy: application to interleukin 1 beta. Biochemistry. 1989;28(15):6150–6.

Masuoka M, Shiraishi H, Ohta S, Suzuki S, Arima K, Aoki S, Toda S, Inagaki N, Kurihara Y, Hayashida S, Takeuchi S, Koike K, Ono J, Noshiro H, Furue M, Conway SJ, Narisawa Y, Izuhara K. Periostin promotes chronic allergic inflammation in response to Th2 cytokines. J Clin Invest. 2012;122(7):2590–600. https://doi.org/10.1172/JCI58978.

Michaylira CZ, Wong GS, Miller CG, Gutierrez CM, Nakagawa H, Hammond R, Klein-Szanto AJ, Lee JS, Kim SB, Herlyn M, Diehl JA, Gimotty P, Rustgi AK. Periostin, a cell adhesion molecule, facilitates invasion in the tumor microenvironment and annotates a novel tumor-invasive signature in

esophageal cancer. Cancer Res. 2010;70(13):5281–92. https://doi.org/10.1158/0008-5472.CAN-10-0704.
Mizejewski GJ. Role of integrins in cancer: survey of expression patterns. Proc Soc Exp Biol Med. 1999;222(2):124–38.
Moody RG, Williamson MP. Structure and function of a bacterial Fasciclin I Domain Protein elucidates function of related cell adhesion proteins such as TGFBIp and periostin. FEBS Open Bio. 2013;3:71–7. https://doi.org/10.1016/j.fob.2013.01.001.
Morra L, Moch H. Periostin expression and epithelial-mesenchymal transition in cancer: a review and an update. Virchows Arch. 2011;459(5):465–75. https://doi.org/10.1007/s00428-011-1151-5.
Palmer AG, Cavanagh J, Wright PE, Rance M. Sensitivity improvement in proton-detected two-dimensional heteronuclear correlation NMR spectroscopy. J Magn Resonan. 1991;93:151–70.
Parulekar AD, Atik MA, Hanania NA. Periostin, a novel biomarker of TH2-driven asthma. Curr Opin Pulm Med. 2014;20(1):60–5. https://doi.org/10.1097/MCP.0000000000000005.
Schrodinger LLC. The PyMOL molecular graphics system, version 1.8; 2015.
Schwieters CD, Kuszewski JJ, Tjandra N, Clore GM. The Xplor-NIH NMR molecular structure determination package. J Magn Reson. 2003;160(1):65–73.
Shao R, Bao SD, Bai XF, Blanchette C, Anderson RM, Dang TY, Gishizky ML, Marks JR, Wang XF. Acquired expression of periostin by human breast cancers promotes tumor angiogenesis through up-regulation of vascular endothelial growth factor receptor 2 expression. Mol Cell Biol. 2004;24(9):3992–4003. https://doi.org/10.1128/Mcb.24.9.3992-4003.2004.
Shen Y, Bax A. Protein backbone and sidechain torsion angles predicted from NMR chemical shifts using artificial neural networks. J Biomol NMR. 2013;56(3):227–41. https://doi.org/10.1007/s10858-013-9741-y.
Suzuki H, Amizuka N, Kii I, Kawano Y, Nozawa-Inoue K, Suzuki A, Yoshie H, Kudo A, Maeda T. Immunohistochemical localization of periostin in tooth and its surrounding tissues in mouse mandibles during development. Anat Rec A Discov Mol Cell Evol Biol. 2004;281(2):1264–75. https://doi.org/10.1002/ar.a.20080.
Tai IT, Dai MR, Chen LB. Periostin induction in tumor cell line explants and inhibition of in vitro cell growth by anti-periostin antibodies. Carcinogenesis. 2005;26(5):908–15. https://doi.org/10.1093/carcin/bgi034.
Takeshita S, Kikuno R, Tezuka K, Amann E. Osteoblast-specific factor 2: cloning of a putative bone adhesion protein with homology with the insect protein fasciclin I. Biochem J. 1993;294(Pt 1):271–8.
Underhaug J, Koldso H, Runager K, Nielsen JT, Sorensen CS, Kristensen T, Otzen DE, Karring H, Malmendal A, Schiott B, Enghild JJ, Nielsen NC. Mutation in transforming growth factor beta induced protein associated with granular corneal dystrophy type 1 reduces the proteolytic susceptibility through local structural stabilization. Biochim Biophys Acta. 2013;1834(12):2812–22. https://doi.org/10.1016/j.bbapap.2013.10.008.
Varner JA, Cheresh DA. Integrins and cancer. Curr Opin Cell Biol. 1996;8(5):724–30.
Wang Z, An J, Zhu D, Chen H, Lin A, Kang J, Liu W, Kang X. Periostin: an emerging activator of multiple signaling pathways. J Cell Commun Signal. 2022;16(4):515–30. https://doi.org/10.1007/s12079-022-00674-2.
Wang Z, Ouyang G. Periostin: a bridge between cancer stem cells and their metastatic niche. Cell Stem Cell. 2012;10(2):111–2. https://doi.org/10.1016/j.stem.2012.01.002.
Ween MP, Oehler MK, Ricciardelli C. Transforming growth factor-beta-induced protein (TGFBI)/(betaig-H3): a matrix protein with dual functions in ovarian cancer. Int J Mol Sci. 2012;13(8):10461–77. https://doi.org/10.3390/ijms130810461.
Wittekind M, Mueller L. HNCACB, a high-sensitivity 3D NMR experiment to correlate amide-proton and nitrogen resonances with the alpha- and beta-carbon resonaces in proteins. J Magn Reson. 1993;101:201–5.
Yun H, Kim EH, Lee CW. (1)H, (13)C, and (15)N resonance assignments of FAS1-IV domain of human periostin, a component of extracellular matrix proteins. Biomol NMR Assign. 2018;12(1):95–8. https://doi.org/10.1007/s12104-017-9786-z.
Yun H, Kim JI, Lee CW. Expression and preparation of periostin FAS1 domains for NMR structure determination. J Korean Magn Resonan Soc. 2016;20(1):17–21. https://doi.org/10.6564/Jkmrs.2016.20.1.017.
Zuiderweg ER, Fesik SW. Heteronuclear three-dimensional NMR spectroscopy of the inflammatory protein C5a. Biochemistry. 1989;28(6):2387–91.

Publisher's Note